IET Image Processing

Research Article

IET Journals
The Institution of Engineering and Technology

Image colourisation by non-local total variation method in the CB and YIQ colour spaces

ISSN 1751-9659
Received on 17th May 2017
Revised 12th August 2017
Accepted on 1st October 2017
E-First on 11th December 2017
doi: 10.1049/iet-ipr.2017.0489
www.ietdl.org

Haibing Hu[1], Fang Li[1] ✉

[1]*Department of Mathematics, East China Normal University, Shanghai, People's Republic of China*
✉ *E-mail: fli@math.ecnu.edu.cn*

Abstract: Colourisation is a process of adding colour to greyscale images. In this study, the authors propose two new colourisation models based on non-local total variation regularisation in the chromaticity and brightness (CB) colour space and the YIQ colour space. Lagrange multiplier method is used to handle the sphere constraint of chromaticity in the CB colour space. By introducing an extra variable and using the dual version of non-local total variation, they split the proposed colourisation problems into two subproblems with closed-form solutions and get two iterative algorithms. Experimental results and comparisons demonstrate that the advantage of the proposed methods is that they can preserve the colour edges better than the closely related existing methods, especially the total variation methods.

1 Introduction

Colourisation is an art of adding colour to grey images or movies. This problem was firstly considered by Fornasier in [1], who insists on recovering paintings in an Italian church which was destroyed in World War II. A major difficulty of colourisation lies in the fact that colourisation may not have the 'correct' answers since the grey image only has one-dimensional (1D) (luminance or intensity) while the colour image involves 3D pixel values. Hence, human interaction may play an important role in the colourisation process which is time consuming and expensive. In recent years, various methods are proposed to solve this problem, which are mainly based on colour transfer, motion estimation, colour prediction, probabilistic relaxation, segmentation, chrominance blending and variational model based methods, see [2, 3, 4, 5, 6, 7, 8, 9, 10, 11] for more details. In this paper, we focus on variational model based methods.

Lagodzinski and Smolka in [12] present a colourisation method which uses the morphological distance transformation and image structures to propagate colour within the greyscale image. Krishnan and Szeliski [13] propose multigrid and multilevel preconditioners to solve image colourisation problems. Uruma *et al.* [14] propose an image colourisation algorithm based on norm minimisation of the mixed l_0/l_1, and they assume that the difference of colour values between neighbour pixels is given as a monotonically increasing function of the difference of grey values between neighbour pixels. Lee *et al.* [15] formulate the colourisation-based compression problem into an optimisation problem by constructing the colourisation matrix in a multiscale manner. Mishiba and Yoshitome [16] propose a colourisation method by constructing a matrix with high compression efficiency and using optimisation for the colourisation-based coding. Pang *et al.* [17] propose a hybrid scheme that combines both the example-based colourisation and the scribble-based colourisation algorithms. Hua *et al.* [18] propose an edge-aware gradient domain optimisation framework filtering by local propagation, which can be used in image colourisation.

Levin *et al.* [9] present a colourisation method in the YIQ colour space which requires neither region tracking nor precise image segmentation. Their basic assumption is that neighbouring pixels in an image with the similar intensities should have the similar colour. Based on this assumption, the user just needs to annotate the image with a few colour scribbles. This method can be used not only in a still image but also image sequences. It is an effective interactive colourisation method in many cases.

Kang and March [10] propose two variational models for image colourisation in the chromaticity and brightness (CB) colour space. The chromaticity component lives on the 2D sphere. To handle the sphere constraint, quadratic penalisation method is adopted to approximate the original problem. The first model is total variation (TV) based which fails in colourisation images with many details. The second model is a modified version of the first model via weighted harmonic map which gives better results than their first model.

Li *et al.* [19] also consider the TV-based colourisation model with sphere constraint in the CB colour space. Different from [10], they introduce the Lagrange multiplier method to handle the sphere constraint which ensures that the chromaticity exactly lives on the sphere. By adding a new variable and using the dual method, they derive an approximate problem in which each subproblem has a closed-form solution.

However, the above mentioned TV or harmonic map based methods in [10, 19] introduce a weight function g to control the speed of colour diffusion, where g is determined by the gradient of the image. In the weak edge areas, g is relatively large. Hence, the colour is easy to diffuse across the edges such that the colour is mixed. To overcome this drawback, we propose to use non-local TV (NLTV) in this work. Instead of g, the non-local weight is used to control the diffusion speed which is determined by the known luminance channel. Experimental results show that the edges of the colour can be better preserved by the proposed method than the TV based methods.

This paper is organised as follows. In Section 2, we introduce the basic conceptions about the CB colour space, the YIQ colour space and NLTV regularisation. In Section 3, we propose the first colourisation method in the CB colour space and derive the iterative algorithm. In Section 4, we propose the second colourisation method in YIQ space and derive the iterative algorithm. In Section 5, we give the numerical experiments and comparisons. Finally, we conclude the paper in Section 6.

2 Preliminaries

In this section, we briefly give the conceptions of the CB colour space, the YIQ colour space [20] and the NLTV regularisation method introduced in [21].

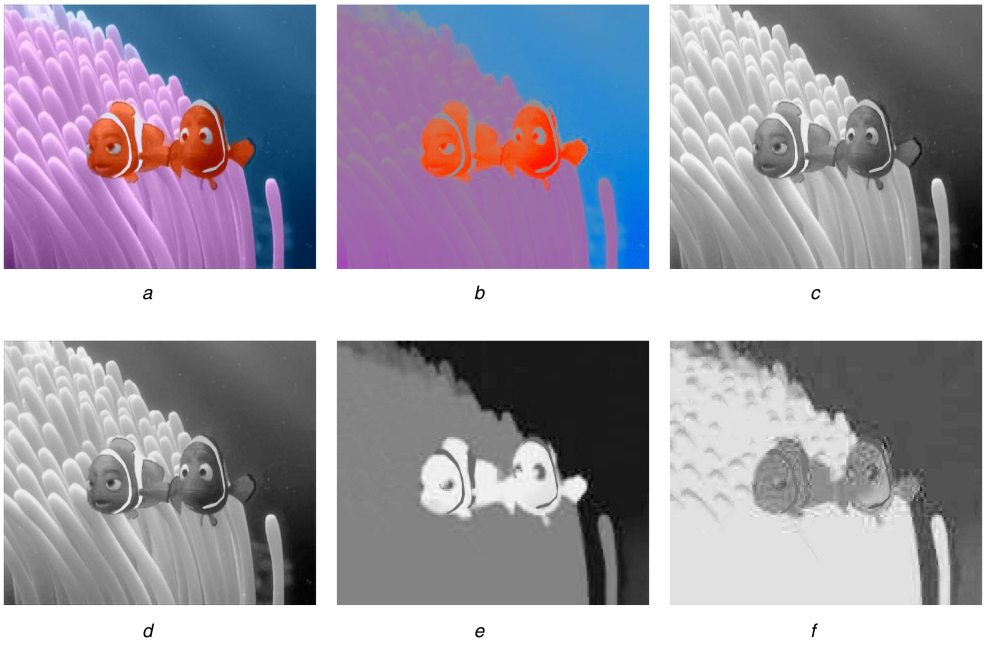

Fig. 1 *Representation of Nemo image in different colour spaces*

(a) Original image in RGB colour space, ***(b)***, ***(c)*** Chromaticity channel C and the brightness channel B, respectively, in the CB colour space, ***(d)–(f)*** Luminance channel Y, and the colour difference channels I and Q, in the YIQ colour space

2.1 CB and YIQ colour spaces

A colour space is a specific organisation of colours. Colour images can be represented in various colour spaces [20]. The typical linear colour models include the red, green and blue (RGB) colour space which is the most widely used; the cyan, magenta, yellow and black (CMYK) colour space which is used in printing; the luminance and two colour difference channels separated colour spaces YCbCr and YIQ, which are widely used in standard colour TV broadcasting and digital video, respectively. Non-linear colour spaces include the hue, saturation, and value (HSV) colour space and the CB colour space, which are close to human colour perception.

In this paper, we use the CB and YIQ colour spaces. Mathematically, assume $\Omega \subset \mathbb{R}^2$ is the image domain, $\boldsymbol{f} = (\boldsymbol{r}, \boldsymbol{g}, \boldsymbol{b}) : \Omega \to \mathbb{R}^3$ is the given colour image in RGB colour space. Then f can be transformed into the CB colour space as

$$\boldsymbol{B} = |\boldsymbol{f}|, \quad \boldsymbol{C} = \boldsymbol{f}/\boldsymbol{B}$$

where $|\cdot|$ is the Euclidean norm, $\boldsymbol{B}$ and $\boldsymbol{C}$ are the brightness and chromaticity components, respectively. Note that the brightness component $\boldsymbol{B}$ is a greyscale image, and the chromaticity component stores the colour information which takes values on the unit sphere S^2 (i.e. $|\boldsymbol{C}| = 1$). The chromaticity component can be regarded as a three-channel image. The linear transform from the RGB colour space to the YIQ colour space is

$$\begin{bmatrix} \boldsymbol{Y} \\ \boldsymbol{I} \\ \boldsymbol{Q} \end{bmatrix} = \begin{bmatrix} 0.299 & 0.587 & 0.114 \\ 0.596 & -0.274 & -0.322 \\ 0.211 & -0.523 & 0.312 \end{bmatrix} \begin{bmatrix} \boldsymbol{R} \\ \boldsymbol{G} \\ \boldsymbol{B} \end{bmatrix}$$

where $\boldsymbol{Y}$ contains the luminance information, $\boldsymbol{I}$ denotes the orange–blue colour change and $\boldsymbol{Q}$ denotes the purple–green colour change.

In Fig. 1, we display one of our test image Nemo in the RGB, CB and YIQ colour spaces, respectively. As can be seen from Figs. 1*c* and *d*, the $\boldsymbol{B}$ channel and $\boldsymbol{Y}$ channel are similar which contain the brightness/luminance information. In Fig. 1*c*, the chromaticity channel $\boldsymbol{C}$ is displayed as a colour image since it contains three channels. Both $\boldsymbol{I}$ and $\boldsymbol{Q}$ are single channels which are displayed as greyscale images in Figs. 1*e* and *f*, respectively. We remark that the single channel images are scaled into [0, 255] for better visual effect. The motivation of this paper is to use the brightness/luminance information contained in $\boldsymbol{B}$ and $\boldsymbol{Y}$ to guide the image colourisation process in the CB and YIQ colour spaces, respectively.

2.2 NLTV regularisation

Assume that $\boldsymbol{u} : \Omega \subset \mathbb{R}^2 \to \mathbb{R}$ is a function. The non-local gradient of $\boldsymbol{u}$ is defined for the pair of points $(x, y) \in \Omega \times \Omega$ as

$$\nabla_\omega \boldsymbol{u}(x, y) = (\boldsymbol{u}(y) - \boldsymbol{u}(x))\sqrt{\boldsymbol{\omega}(x, y)} : \Omega \times \Omega \to \mathbb{R},$$

where $\boldsymbol{\omega} : \Omega \times \Omega \to \mathbb{R}_+$ is the weight between the points x, y and ∇_ω denotes the non-local gradient. The inner product between two non-local vectors $\boldsymbol{p}_1, \boldsymbol{p}_2 : \Omega \times \Omega \to \mathbb{R}$ at point $x \in \Omega$ is defined as

$$\langle \boldsymbol{p}_1, \boldsymbol{p}_2 \rangle(x) = \int_\Omega \boldsymbol{p}_1(x, y) \boldsymbol{p}_2(x, y)\, \mathrm{d}y : \Omega \to \mathbb{R}$$

which induces the norm of a non-local vector $\boldsymbol{p} : \Omega \times \Omega \to \mathbb{R}$ at point $x \in \Omega$ as follows:

$$|\boldsymbol{p}|(x) = \sqrt{\int_\Omega \boldsymbol{p}(x, y)^2\, \mathrm{d}y} : \Omega \to \mathbb{R}_+.$$

Then the norm of the non-local gradient of a function $u : \Omega \to \mathbb{R}$ at $x \in \Omega$ is given by

$$|\nabla_\omega \boldsymbol{u}|(x) = \sqrt{\int_\Omega (\boldsymbol{u}(y) - \boldsymbol{u}(x))^2 \boldsymbol{\omega}(x, y)\, \mathrm{d}y} : \Omega \to \mathbb{R}_+.$$

The non-local divergence operator can be defined by the standard adjoint relation with the non-local gradient

$$\langle \nabla_\omega \boldsymbol{u}, \boldsymbol{p} \rangle = -\langle \boldsymbol{u}, \mathrm{div}_\omega \boldsymbol{p} \rangle,$$

$\forall \boldsymbol{u} : \Omega \to \mathbb{R}, \forall \boldsymbol{p} : \Omega \times \Omega \to \mathbb{R}$, which defines the non-local divergence of the non-local vector $\boldsymbol{p} : \Omega \times \Omega \to \mathbb{R}$ at $x \in \Omega$:

$$\mathrm{div}_\omega \boldsymbol{p}(x) = \int_\Omega (\boldsymbol{p}(x,y) - \boldsymbol{p}(y,x))\sqrt{\boldsymbol{\omega}(x,y)}\,\mathrm{d}y : \Omega \to \mathbb{R}\,.$$

See [21, 22] for more details.

For the image denoising problem, Gilboa and Osher [21] propose to use NLTV regularisation (defined as $\int_\Omega |\nabla_\omega \boldsymbol{u}|$) in the following model:

$$\inf_{\boldsymbol{u}} F(\boldsymbol{u}) = \int_\Omega |\nabla_\omega \boldsymbol{u}| + \frac{\lambda}{2}(\boldsymbol{u} - \boldsymbol{u}_0)^2\,\mathrm{d}x, \tag{1}$$

where $\boldsymbol{u}_0$ is the given noisy image, $\boldsymbol{u}$ is the desired clean image, and $\lambda > 0$ is a balance parameter. In image denoising, the NLTV model greatly outperforms the TV model in the aspect of fine structure preserving. NLTV regularisation is generalised to image deconvolution, compressed sensing and wavelet inpainting [23, 24].

In order to take use of the advantage of NLTV, we propose to use NLTV as a regularisation term in the image colourisation problem. Moreover, it is reasonable to consider NLTV in image colourisation since similar patches are likely to have similar colours.

3 Proposed method in the CB colour space

In this section, we propose the first variational model for image colourisation based on NLTV in the CB colour space. Then an iterative algorithm is derived based on the Lagrange multiplier method and the operator splitting technique.

Let $D \subset \Omega$ be the colourisation domain where the colour information is missing, and $D^c = \Omega \backslash D$ be the complement of Ω where the colour is given.

3.1 Model in the CB colour space

We assume that the brightness component B is known. Image colourisation in the CB colour space aims to recover the missing chromaticity information $\boldsymbol{C}$ in the colour missing domain D. We propose the following constrained model for image colourisation:

$$\inf_{|\boldsymbol{C}| = 1} E(\boldsymbol{C}) = \int_\Omega |\nabla_\omega \boldsymbol{C}|\,\mathrm{d}x + \frac{1}{2}\int_\Omega \hat{\lambda}|\boldsymbol{C} - \boldsymbol{C}_0|^2\,\mathrm{d}x, \tag{2}$$

where

$$\hat{\lambda} = \begin{cases} \lambda, & x \in D^c \\ 0, & x \in D \end{cases} \tag{3}$$

In the model (2), $\boldsymbol{C}$ denotes the chromaticity component, $\boldsymbol{C}_0$ is the given chromaticity, $\lambda > 0$ is a given parameter, $\omega(x,y)$ is the non-local weight, and $|\nabla_\omega \boldsymbol{C}| := \sum_{k=1}^3 |\nabla_\omega \boldsymbol{C}_k|$ where $\boldsymbol{C}_k$ is the kth channel of the chromaticity. Note that C_0 is only given in D^c. For the convenience of computation, we extend the values of $\boldsymbol{C}_0$ to the colour missing region D as $(1/\sqrt{3}, 1/\sqrt{3}, 1/\sqrt{3})$ in order to satisfy the sphere constraint.

The weight $\omega(x,y)$ plays an important role in the proposed method. Different from the NLTV denoising method where w is decided by the noisy image [23], in our method we use the known brightness channel $\boldsymbol{B}$ to define the weight. We denote $P_x(B)$ as the patch of size $(2m+1) \times (2m+1)$ centred at a pixel $x \in \Omega$ in the brightness image $\boldsymbol{B}$

$$P_x(\boldsymbol{B})(t) = \boldsymbol{B}(x+t), t = [-m, \ldots, m]^2,$$

where m is the half patch size, t is the pixel position in the patch and $P_x(B)(t)$ is the pixel value at position t in the patch. As a variant method of [23], we define the weight between two points x and y as a function of the patch distance in the $\boldsymbol{B}$ channel

$$\omega(B)(x,y) = \mathrm{e}^{-(\|P_x(B) - P_y(B)\|_F^2)/2h^2)}, \tag{4}$$

where h is a filtering parameter and $\|\cdot\|_F$ denotes the Frobenius norm of a matrix. To reduce the computational complexity, we search for the similar patches of $P_x(B)$ only in the non-local window centred at x with window size $(2s+1) \times (2s+1)$ where $s > m$.

Let us give some explanations of the proposed model (2). The first term is the NLTV regularisation term which requires that the recovered channel $\boldsymbol{C}$ should be smooth with a small NLTV value. In other words, it requires that the centre pixels of similar patches have similar chromaticity, which seems reasonable. The second term is the data-fitting term which requires that the chromaticity component $\boldsymbol{C}$ should be close to $\boldsymbol{C}_0$ in D^c. The two terms are balanced by the parameter λ. Remark that the proposed model (2) is different from the model (1) in three aspects. Firstly, in (1) the fidelity parameter is a scalar, while in our model it is a function which indicates the area with colour. Secondly, the definition of weight is essentially different since in (1) the noisy image is used to calculate the distance while in our model the known B channel is used in the calculation. Thirdly, in our method $\boldsymbol{C}$ is constrained to be on the sphere, i.e. $|\boldsymbol{C}| = 1$.

3.2 Algorithm in the CB colour space

In this section, we derive the algorithm of the proposed method. By introducing an extra variable $\tilde{\boldsymbol{C}}$, we approximate the problem (1) by the following problem:

$$\begin{aligned} \inf_{\boldsymbol{C}, |\tilde{\boldsymbol{C}}| = 1} E_\theta(\boldsymbol{C}, \tilde{\boldsymbol{C}}) &= \int_\Omega |\nabla_\omega \boldsymbol{C}|\,\mathrm{d}x + \frac{\theta}{2}\int_\Omega |\boldsymbol{C} - \tilde{\boldsymbol{C}}|^2\,\mathrm{d}x \\ &+ \frac{1}{2}\int_\Omega \hat{\lambda}(\tilde{\boldsymbol{C}} - \boldsymbol{C}_0)^2\,\mathrm{d}x \end{aligned} \tag{5}$$

where θ is big enough to ensure that $\tilde{\boldsymbol{C}}$ is close to $\boldsymbol{C}$. Then we use the Lagrange multiplier method and relax the constraints in the approximate problem (5) as

$$\inf_{\boldsymbol{C}, \tilde{\boldsymbol{C}}, \mu} \left\{ \begin{aligned} E_\theta(\boldsymbol{C}, \tilde{\boldsymbol{C}}) &= \int_\Omega |\nabla_\omega \boldsymbol{C}|\,\mathrm{d}x + \frac{\theta}{2}\int_\Omega |\boldsymbol{C} - \tilde{\boldsymbol{C}}|^2\,\mathrm{d}x \\ &+ \frac{1}{2}\int_\Omega \hat{\lambda}(\tilde{\boldsymbol{C}} - \boldsymbol{C}_0)^2\,\mathrm{d}x + \frac{1}{2}\int_\Omega \mu(|\tilde{\boldsymbol{C}}|^2 - 1)\,\mathrm{d}x \end{aligned} \right\} \tag{6}$$

where $\boldsymbol{\mu}(x)$ is the Lagrange multiplier at pixel x which corresponds to the constraint $|\tilde{\boldsymbol{C}}(x)| = 1$.

The above unconstrained approximate problem (6) can be decomposed into two subproblems

$$\begin{aligned} \inf_{\tilde{\boldsymbol{C}}, \mu} &\frac{\theta}{2}\int_\Omega |\boldsymbol{C} - \tilde{\boldsymbol{C}}|^2\,\mathrm{d}x + \frac{1}{2}\int_\Omega \hat{\lambda}(\tilde{\boldsymbol{C}} - \boldsymbol{C}_0)^2\,\mathrm{d}x \\ &+ \frac{1}{2}\int_\Omega \boldsymbol{\mu}(|\tilde{\boldsymbol{C}}|^2 - 1)\,\mathrm{d}x \end{aligned} \tag{7}$$

$$\inf_{\boldsymbol{C}} \int_\Omega |\nabla_\omega \boldsymbol{C}|\,\mathrm{d}x + \frac{\theta}{2}\int_\Omega |\boldsymbol{C} - \tilde{\boldsymbol{C}}|^2\,\mathrm{d}x \tag{8}$$

In the first subproblem (7), by taking the derivative of energy in (7) with respect to $\tilde{\boldsymbol{C}}$ and setting the result to zero, we have

$$\theta(\tilde{\boldsymbol{C}} - \boldsymbol{C}) + \hat{\lambda}(\tilde{\boldsymbol{C}} - \boldsymbol{C}_0) + \mu\tilde{\boldsymbol{C}} = 0. \tag{9}$$

Multiplying (9) by vector $\tilde{\boldsymbol{C}}$ and using the constraint $|\tilde{\boldsymbol{C}}|^2 = 1$ yields

$$\boldsymbol{\mu}(x) = \theta\langle\tilde{\boldsymbol{C}}, \boldsymbol{C}\rangle + \hat{\lambda}\langle\tilde{\boldsymbol{C}}, \boldsymbol{C}_0\rangle - \theta - \hat{\lambda} \tag{10}$$

where $\langle\tilde{\boldsymbol{C}}(x), \boldsymbol{C}(x)\rangle := \sum_{k=1}^3 \tilde{\boldsymbol{C}}_k(x)\boldsymbol{C}_k(x)$ denotes the inner product of vectors in $\mathbb{R}^3$. From (9) and (10), the solution of $\tilde{\boldsymbol{C}}$ is given by the following formula:

$$\tilde{\boldsymbol{C}} = \frac{\theta \boldsymbol{C} + \hat{\boldsymbol{\lambda}} \boldsymbol{C}_0}{\theta + \hat{\boldsymbol{\lambda}} + \boldsymbol{\mu}}. \tag{11}$$

For fixed $\tilde{\boldsymbol{C}}$, the second subproblem (8) is the NLTV denoising problem for vector-valued images. In the following, we use the dual version of NLTV to derive the numerical scheme for this subproblem, which is a generalisation in the case of TV denoising for greyscale image [25]. As shown by Chan *et al.* [26], the dual version of the problem (8) about $\boldsymbol{C}$ is equivalent to the following dual min–max problem:

$$\inf_{\boldsymbol{C}} \sup_{|\boldsymbol{p}| \le 1} \int_\Omega \langle \nabla_\omega \boldsymbol{C}, \boldsymbol{p} \rangle + \frac{\theta}{2} |\boldsymbol{C} - \tilde{\boldsymbol{C}}|^2 \, \mathrm{d}x \tag{12}$$

where $\nabla_\omega \boldsymbol{C}$, $\boldsymbol{p} = (p_1, p_2, p_3): \Omega \times \Omega \to \mathbb{R}^3$ are non-local vectors. According to the mini–max theorem in [27], the *inf* and *sup* can be swapped here since the functional in (12) is convex in $\boldsymbol{C}$ and concave in $\boldsymbol{p}$. Hence we get that (12) is equivalent to

$$\sup_{|\boldsymbol{p}| \le 1} \inf_{\boldsymbol{C}} \int_\Omega \langle \boldsymbol{C}, \operatorname{div}_\omega \boldsymbol{p} \rangle + \frac{\theta}{2} |\boldsymbol{C} - \tilde{\boldsymbol{C}}|^2 \, \mathrm{d}x, \tag{13}$$

where the non-local divergence operator for vectors is defined as $\operatorname{div}_\omega \boldsymbol{p} := (\operatorname{div}_\omega \boldsymbol{p}_1, \operatorname{div}_\omega \boldsymbol{p}_2, \operatorname{div}_\omega \boldsymbol{p}_3)$. The Euler–Lagrange equation about $\boldsymbol{C}$ is

$$\operatorname{div}_\omega \boldsymbol{p} + \theta(\boldsymbol{C} - \tilde{\boldsymbol{C}}) = 0.$$

Then the solution of $\boldsymbol{C}$ is given by

$$\boldsymbol{C} = \tilde{\boldsymbol{C}} - \operatorname{div}_\omega \boldsymbol{p} / \theta. \tag{14}$$

Substituting (14) into (13), we get the following problem of $\boldsymbol{p}$:

$$\sup_{|\boldsymbol{p}| \le 1} \int_\Omega \langle \theta \tilde{\boldsymbol{C}}, \operatorname{div}_\omega \boldsymbol{p} \rangle - \frac{1}{2} |\operatorname{div}_\omega \boldsymbol{p}|^2 \, \mathrm{d}x.$$

By the Lagrange multipliers method, the constrained problem is changed to the following unconstrained problem:

$$\sup \int_\Omega \langle \theta \tilde{\boldsymbol{C}}, \operatorname{div}_\omega \boldsymbol{p} \rangle + \frac{\alpha}{2} (|\boldsymbol{p}|^2 - 1) - \frac{1}{2} |\operatorname{div}_\omega \boldsymbol{p}|^2 \, \mathrm{d}x.$$

The Euler–Lagrange equation about $\boldsymbol{p}$ is

$$-(\nabla_\omega (\operatorname{div}_\omega \boldsymbol{p} - \theta \tilde{\boldsymbol{C}})) + \alpha \boldsymbol{p} = 0,$$

where either $|\alpha| > 0$ and $|\boldsymbol{p}| = 1$, or $\alpha = 0$ and $|\boldsymbol{p}| < 1$. In the latter case, it holds that $\nabla_\omega (\operatorname{div}_\omega \boldsymbol{p} - \theta \tilde{\boldsymbol{C}}) = 0$. Then, we have that in any case

$$\alpha = |\nabla_\omega (\operatorname{div}_\omega \boldsymbol{p} - \theta \tilde{\boldsymbol{C}})|.$$

Choosing $\tau > 0$ and letting $\boldsymbol{p}^0 = 0$, for any $k > 0$, we thus use the following semi-implicit gradient descent algorithm of $\boldsymbol{p}$:

$$\boldsymbol{p}^{k+1} = \frac{\boldsymbol{p}^k + \tau \nabla_\omega (\operatorname{div}_\omega \boldsymbol{p}^k - \theta \tilde{\boldsymbol{C}})}{1 + \tau |\nabla_\omega (\operatorname{div}_\omega \boldsymbol{p}^k - \theta \tilde{\boldsymbol{C}})|}. \tag{15}$$

Based on the formulas (10), (11), (14) and (15), we summarise the proposed NLTV colourisation algorithm in the CB colour space in Algorithm 1 (NLTV_CB for short). Note that in Algorithm 1, $\theta > 0$ is a given parameter and $k_{\max}$ is the maximum iteration defined by the user.

Algorithm 1: NLTV_CB colourisation algorithm

1. Initialisation: $\boldsymbol{p}^0 = \boldsymbol{0}$, $\tau = 0.5$, $\tilde{\boldsymbol{C}}^0 = \boldsymbol{C}_0$, $\theta > 0$;
2. Iteration: for $k = 0, 1, 2, \ldots$

$$\boldsymbol{p}^{k+1} = \frac{\boldsymbol{p}^k + \tau \nabla_\omega (\operatorname{div}_\omega \boldsymbol{p}^k - \theta \tilde{\boldsymbol{C}}^k)}{1 + \tau |\nabla_\omega (\operatorname{div}_\omega \boldsymbol{p}^k - \theta \tilde{\boldsymbol{C}}^k)|},$$

$$\boldsymbol{C}^{k+1} = \tilde{\boldsymbol{C}}^k - \operatorname{div}_\omega \boldsymbol{p}^{k+1} / \theta,$$

$$\boldsymbol{\mu}^{k+1} = \theta \langle \tilde{\boldsymbol{C}}^k, \boldsymbol{C}^{k+1} \rangle + \hat{\boldsymbol{\lambda}} \langle \tilde{\boldsymbol{C}}^k, \boldsymbol{C}_0 \rangle - \theta - \hat{\boldsymbol{\lambda}},$$

$$\tilde{\boldsymbol{C}}^{k+1} = \frac{\theta \boldsymbol{C}^{k+1} + \hat{\boldsymbol{\lambda}} \boldsymbol{C}_0}{\theta + \hat{\boldsymbol{\lambda}} + \boldsymbol{\mu}^{k+1}},$$

3. Termination criterion: $k > k_{\max}$.

4 Proposed method in the YIQ colour space

For image colourisation problem in the YIQ colour space, the luminance channel $\boldsymbol{Y}$ is assumed to be known. Hence one need only to recover the other two colour channels, namely, $\boldsymbol{I}$ and $\boldsymbol{Q}$. Note that the YIQ colour space is also used in [9, 28]. We make use of the information of $\boldsymbol{Y}$ channel to guide the colourisation process of $\boldsymbol{I}$ and $\boldsymbol{Q}$ channels.

Let $\boldsymbol{C}$ denotes the colour difference channel $\boldsymbol{I}$ or $\boldsymbol{Q}$, $\boldsymbol{C}_0$ is the given colour information in the $\boldsymbol{I}$ or $\boldsymbol{Q}$ channel and $\lambda > 0$ is a given parameter. We propose the second model for image colourisation

$$\inf_{\boldsymbol{C}} E(\boldsymbol{C}) = \int_\Omega |\nabla_\omega \boldsymbol{C}| \, \mathrm{d}x + \frac{1}{2} \int_\Omega \hat{\boldsymbol{\lambda}} |\boldsymbol{C} - \boldsymbol{C}_0|^2 \, \mathrm{d}x, \tag{16}$$

where the parameter $\hat{\boldsymbol{\lambda}}$ is defined by (3) and the non-local weight $\boldsymbol{\omega}$ is defined as in (4) by replacing $\boldsymbol{B}$ with $\boldsymbol{Y}$.

Remark that the model (16) is different from the model (2) in the two aspects. Firstly, the model (16) is componentwise since $\boldsymbol{I}$ and $\boldsymbol{Q}$ are processed separately. Secondly, the model (16) is unconstrained. Hence solving the model (16) is easier than solving the model (2).

By introducing an extra variable $\tilde{\boldsymbol{C}}$, we approximate the problem (16) by the following problem:

$$\inf_{\boldsymbol{C}, \tilde{\boldsymbol{C}}} \int_\Omega |\nabla_\omega \boldsymbol{C}| \, \mathrm{d}x + \frac{\theta}{2} \int_\Omega |\boldsymbol{C} - \tilde{\boldsymbol{C}}|^2 \, \mathrm{d}x + \frac{1}{2} \int_\Omega \hat{\boldsymbol{\lambda}} (\tilde{\boldsymbol{C}} - \boldsymbol{C}_0)^2 \, \mathrm{d}x \tag{17}$$

where θ is big enough to ensure that $\tilde{\boldsymbol{C}}$ is close to $\boldsymbol{C}$. Then $\boldsymbol{C}$ and $\tilde{\boldsymbol{C}}$ can be solved by the alternating minimisation method.

For fixed $\boldsymbol{C}$, it is easy to get the solution of $\tilde{\boldsymbol{C}}$:

$$\tilde{\boldsymbol{C}} = \frac{\theta \boldsymbol{C} + \hat{\boldsymbol{\lambda}} \boldsymbol{C}_0}{\theta + \hat{\boldsymbol{\lambda}}}. \tag{18}$$

For fixed $\tilde{\boldsymbol{C}}$, the subproblem for $\boldsymbol{C}$ is the standard NLTV denoising problem

$$\inf_{\boldsymbol{C}} \int_\Omega |\nabla_\omega \boldsymbol{C}| \, \mathrm{d}x + \frac{\theta}{2} \int_\Omega |\boldsymbol{C} - \tilde{\boldsymbol{C}}|^2 \, \mathrm{d}x. \tag{19}$$

The solution can be derived by a similar deduction as in Section 3. Based on formulas (14), (15) and (18), we can summarise the proposed NLTV colourisation algorithm in the YIQ colour space in Algorithm 2 (NLTV_YIQ for short).

Algorithm 2: NLTV_YIQ colourisation algorithm

1. Initialisation: $\boldsymbol{p}^0 = \boldsymbol{0}$, $\tau = 0.5$, $\tilde{\boldsymbol{C}}^0 = \boldsymbol{C}_0$, $\theta > 0$;
2. Iteration: for $k = 0, 1, 2, \ldots$

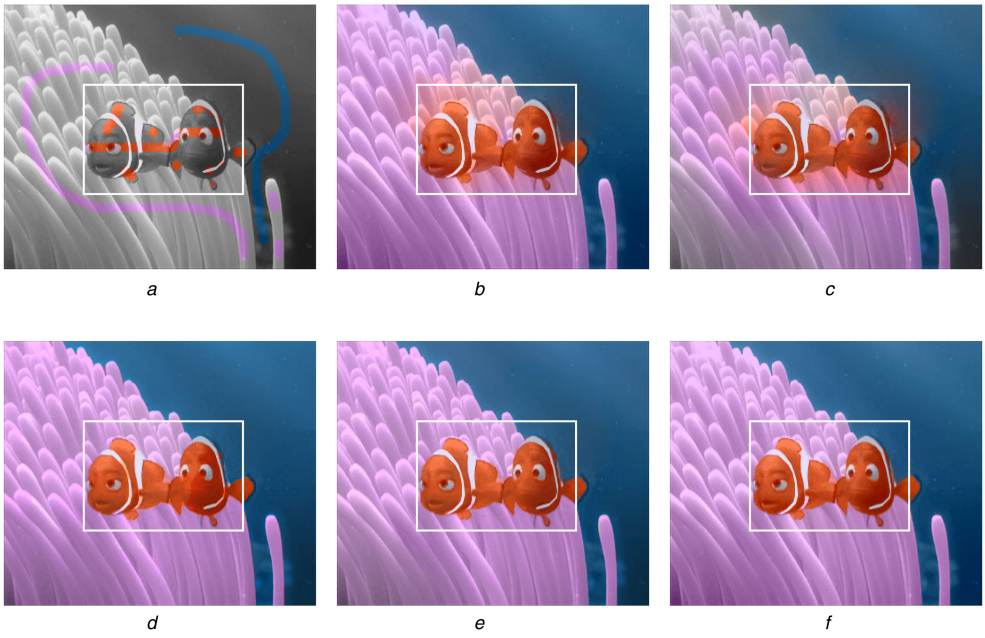

Fig. 2 *Colourisation results by different methods on Nemo image*

(a) Marked image, ***(b)*** Result of [9], PSNR = 28.67 dB, ***(c)*** Result of [10], PSNR = 22.18 dB, ***(d)*** Result of [19], PSNR = 29.14 dB, ***(e)*** Result of the proposed method NLTV_CB, PSNR = 30.20 dB (parameters: $h = 40^{-1}$, $\theta^{-1} = 0.04$), ***(f)*** Result of the proposed method NLTV_YIQ, PSNR = 32.46 dB (parameter: $h = 40^{-1}$)

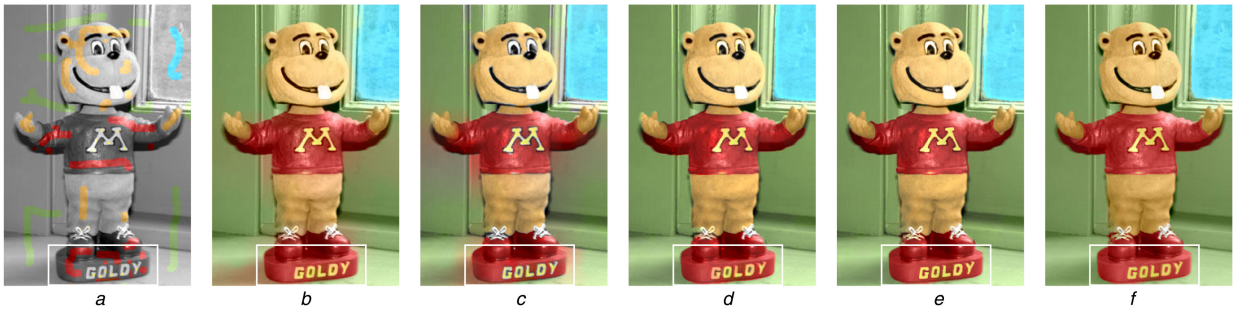

Fig. 3 *Colourisation results by different methods on Goldy image*

(a) Marked image, ***(b)*** Result of [9], PSNR = 30.00 dB, ***(c)*** Result of [10], PSNR = 25.63 dB, ***(d)*** Result of [19], PSNR = 29.11 dB, ***(e)*** Result of the proposed method NLTV_CB, PSNR = 30.30 dB (parameter: $\theta^{-1} = 0.03$), ***(f)*** Result of the proposed method NLTV_YIQ, PSNR = 30.60 dB (parameter: $\theta^{-1} = 0.03$)

$$\boldsymbol{p}^{k+1} = \frac{\boldsymbol{p}^k + \tau\nabla_\omega(\mathrm{div}_\omega \boldsymbol{p}^k - \theta\tilde{\boldsymbol{C}}^k)}{1 + \tau|\nabla_\omega(\mathrm{div}_\omega \boldsymbol{p}^k - \theta\tilde{\boldsymbol{C}}^k)|},$$

$$\boldsymbol{C}^{k+1} = \tilde{\boldsymbol{C}}^k - \mathrm{div}_\omega \boldsymbol{p}^{k+1}/\theta,$$

$$\tilde{\boldsymbol{C}}^{k+1} = \frac{\theta\boldsymbol{C}^{k+1} + \hat{\lambda}\boldsymbol{C}_0}{\theta + \hat{\lambda}},$$

3. Termination criterion: $k > k_{\max}$.

5 Experiments and comparisons

In this section, we compare our methods with three closely related methods including the optimisation based methods in [9] and the TV based methods in [10, 19]. All the experiments are performed under Windows 8 and MATLAB R2012a with Intel Core i7-4500 CPU@1.80 GHz and 8 GB memory. The test images are Nemo, Goldy, Peppers, and Shirley as shown in Figs. 2*a*, 3*a*, 4*a* and 5*a*, in which some colour scribbles are given. The maximum iteration numbers of the methods in [10, 19] are set as 20,000 and 500, respectively. For a fair comparison, the other parameters in each method are tuned in order to get the optimal results for each image. In our experiments, unless otherwise specified, the default setting of parameters for our methods is

$$\lambda = 10000, \quad m = 5, \quad s = 10, \quad h = 30^{-1}, \quad \theta^{-1} = 0.05, \quad k_{\max} = 1000.$$

Here λ is the fidelity parameter in (3), m is the patch window radius, s is the search window radius, and h is the filtering parameter in the non-local weight defined in (4). The parameter θ^{-1} controls the extent of NLTV regularisation in (8), or equivalently, the diffusion speed. Generally, bigger θ^{-1} means faster colourisation speed, however, bigger θ^{-1} also tends to result in colour blending phenomena across the edges. Hence the choice of a suitable θ is important.

In Figs. 2*b–f*, we display the numerical results on Nemo image by different methods. For a detailed comparison, we enlarge the white rectangle areas in the images in Figs. 6*b–f*. It can be seen that in Figs. 2*b*, *c* and 6*b*, *c*, the methods in [9, 10] lead to colour diffusion across the edges of Nemo's body such that the colour blending phenomenon occurs in some regions. The result by the method in [19] seems better, as shown in Fig. 2*d*. However, in the enlarged region, as displayed in Fig. 6*d*, the colour blending phenomenon also occurs along the white stripes on Nemo. By contrast, the colourisation results of our methods are much clearer than the others with almost no colour blending phenomenon, as shown in Figs. 2*e* and *f* and the enlarged details shown in Figs. 6*e* and *f*.

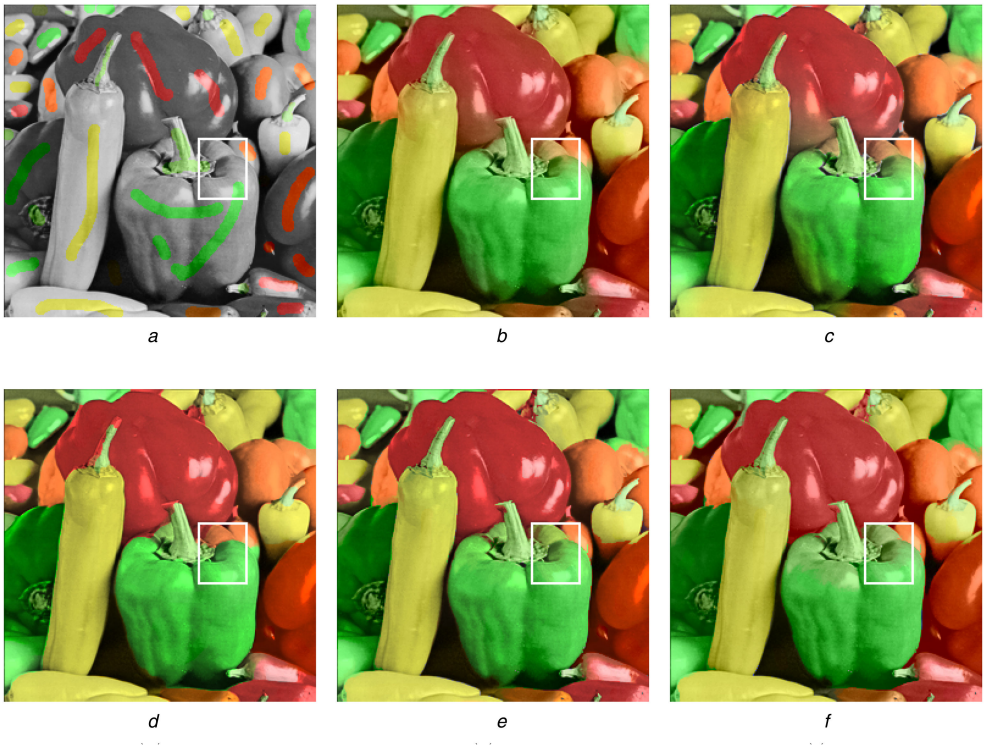

Fig. 4 *Colourisation results by different methods on Peppers image*
(a) Marked image, ***(b)*** Result of [9], ***(c)*** Result of [10], ***(d)*** Result of [19],
(e) Result of the proposed method NLTV_CB (parameter: $h = 40^{-1}$),
(f) Result of the proposed method NLTV_YIQ

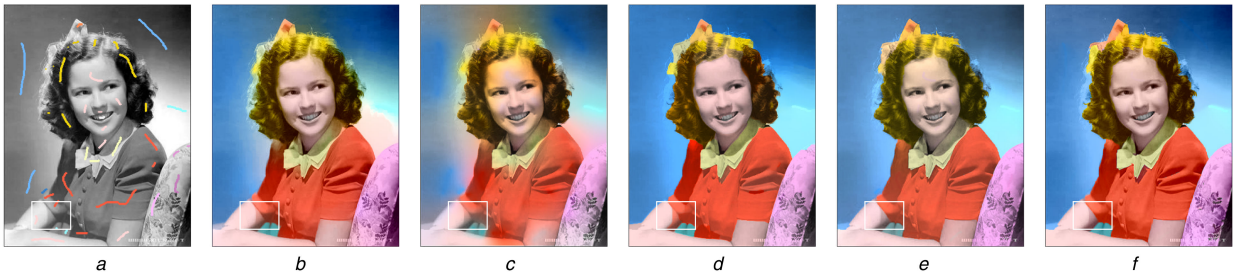

Fig. 5 *Colourisation results by different methods on Shirley image*
(a) Marked image, ***(b)*** Result of [9], ***(c)*** Result of [10], ***(d)*** Result of [19],
(e) Result of the proposed method NLTV_CB (parameters: $m = 2, s = 3, h = 50^{-1}, \theta = 0.09$),
(f) Result of the proposed method NLTV_YIQ (parameters: $m = 1, s = 3, \theta = 0.05$)

Fig. 3 shows the results on Goldy image by different methods. We can see that in the results by the methods in [9, 10, 19] the colour blending phenomenon occurs. While in the results by the proposed methods, the colour edges are better preserved than others. In particular, the text area with 'GOLDY' is enlarged for detail comparison in Fig. 7. It is obvious that the proposed methods keep the letters much better than others.

In Fig. 4, we display the colourisation results on Peppers image by different methods. The colour blending effect can also be observed in the results by the methods in [9, 10, 19]. The proposed method can preserve the edges of colour better. In particular, in the enlarged region as displayed in Fig. 8, it is obvious that the colourisation results by methods in [9, 10, 19] are not reasonable for the front pepper since it is expected to be in green colour. By contrast, the results by the proposed methods are more reasonable and satisfactory.

Fig. 5 shows the colourisation results on Shirley image by different methods. The colour blending effect is obvious in the results by the methods in [9, 10]. The results of the other three methods seem similar. However, by careful comparison of the zoomed arm regions in Fig. 9, we find that our methods give more satisfactory results in the shadow of the arm than others.

By the visual comparison in Figs. 2–9, we can conclude that the proposed methods can prevent the colour blending effect in the process of colourisation and can preserve the edges of the colour well especially in the slenderness areas. For quantitative comparison, we use the peak signal-to-noise ratio (PSNR) index for colour image as a measure, which is defined by

$$\mathrm{PSNR} = 10\log_{10}\left(\frac{255^2 \cdot 3N}{\sum_{(i,j,k)} |\boldsymbol{X}_{ijk} - \boldsymbol{Y}_{ijk}|^2}\right),$$

where (i, j) denotes the pixel location, $k = 1,2,3$ denotes the channel, N is the total number of pixels, $\boldsymbol{X}$ is the ground truth image, and $\boldsymbol{Y}$ is the computed result image. Since the ground truth images of Nemo and Goldy are available, we can compare the PSNR values of the result by each method for them. The PSNR values are reported in Figs. 2 and 3. Among all the compared methods, the method in [10] has the lowest PSNR values. The methods in [9, 19] gain much higher PSNR values than the method in [10]. The proposed methods outperform the others in terms of PSNR values. Moreover, the proposed method NLTV_YIQ has higher PSNR values than the proposed method NLTV_CB.

In Figs. 10, we display the intermediate results of our method NLTV_CB on Nemo image. From the left to the right are the brightness components, the initial chromaticity components with marks and the colourised chromaticity components. In Fig. 10*c*, it

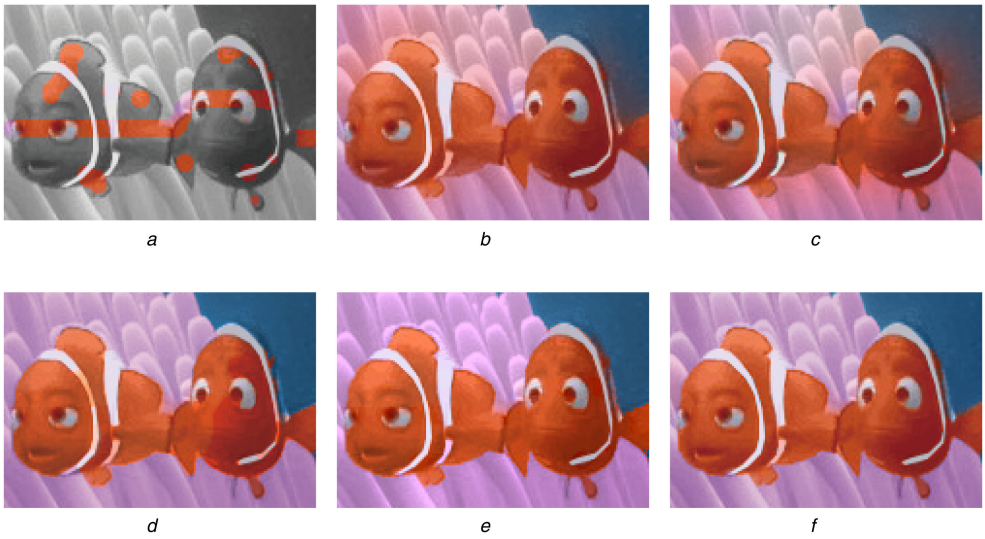

Fig. 6 *Enlarged rectangle regions of Figs. 2a–f, respectively*

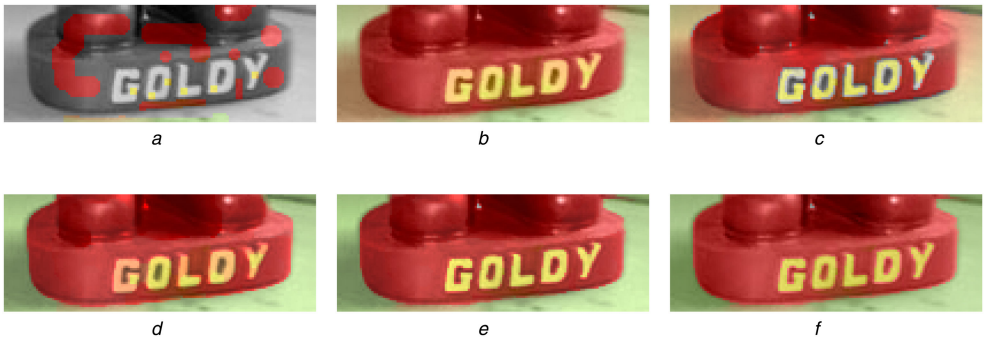

Fig. 7 *Enlarged rectangle regions of Figs. 3a–f, respectively*

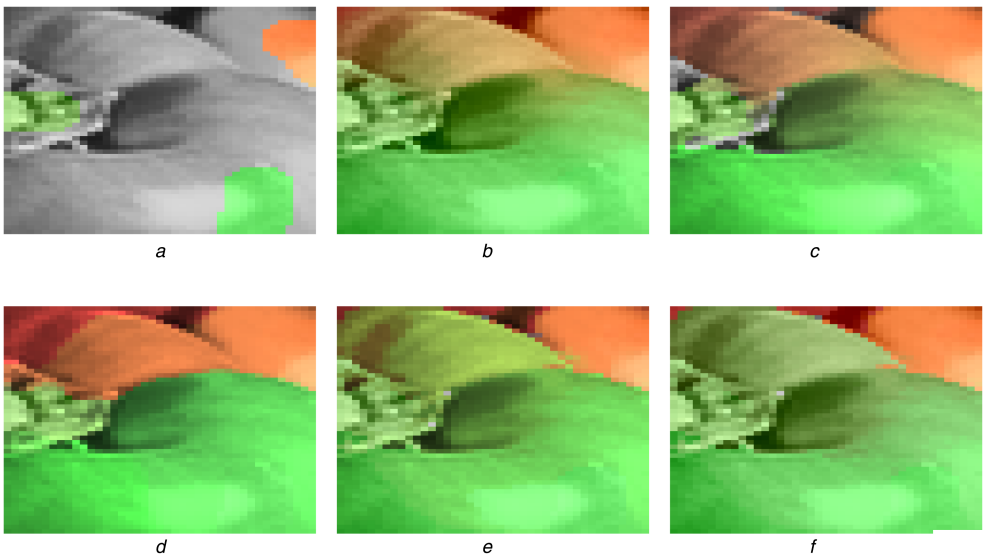

Fig. 8 *Enlarged rectangle regions of Figs. 4a–f, respectively*

is obvious that the colour edges are well preserved by our method NLTV_CB.

In Figs. 11, we show the initial $\boldsymbol{Y}$, $\boldsymbol{I}$, $\boldsymbol{Q}$ channels and the colourised $\boldsymbol{I}$, $\boldsymbol{Q}$ channels by our method NLTV_YIQ for Nemo image. From the results of $\boldsymbol{I}$ and $\boldsymbol{Q}$ channels in the second row, we find that the proposed method can preserve the edges in the $\boldsymbol{I}$ and $\boldsymbol{Q}$ channels well while diffusing the colour information. Therefore our method can preserve the colour edges well

To compare the computational efficiency, we take Nemo image with size 264×324 as an example. The method in [9] needs no iteration and it takes about 8 s to finish the colourisation process. The other three methods are iterative methods and are more time consuming. The method in [10] takes about 464 s for 20,000 iterations, the method in [19] takes about 13 s for 500 iterations, the proposed method NLTV_CB takes about 162 s for 1000 iterations and the proposed method NLTV_YIQ takes about 77 s

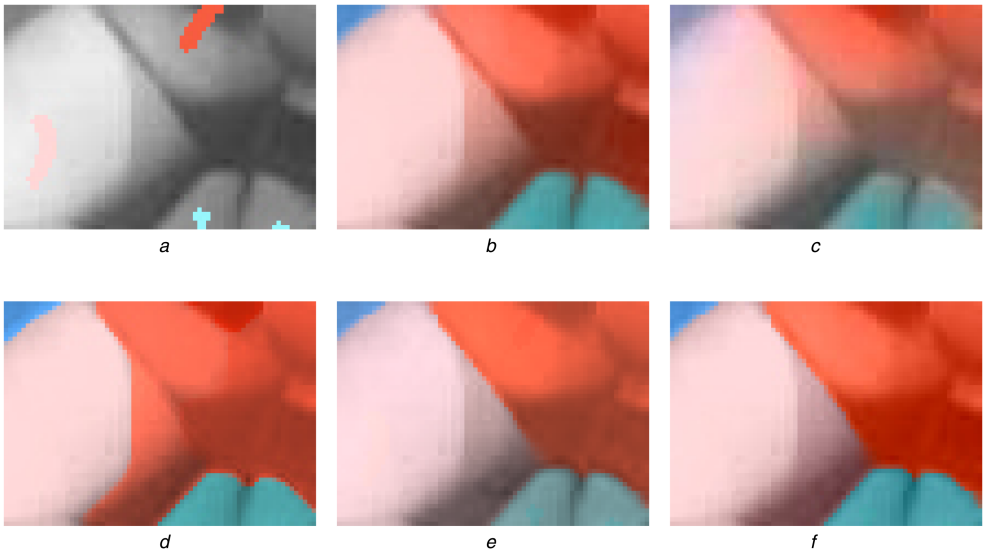

Fig. 9 *Enlarged rectangle regions of Figs. 5a–f, respectively*

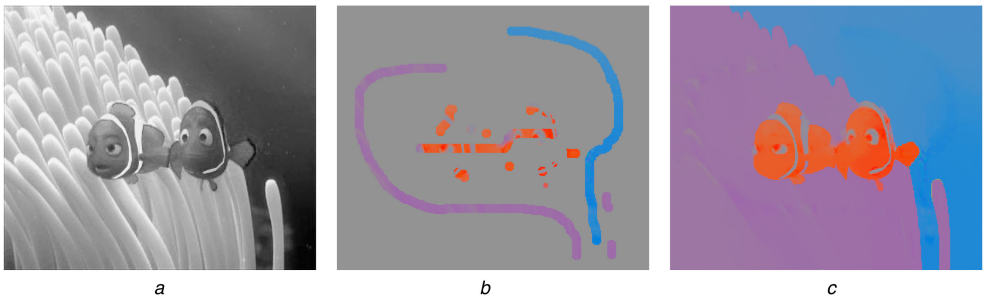

Fig. 10 *Intermediate colourisation results of the proposed method NLTV_CB on Nemo image*
(a) Given brightness components,
(b) Initial marked chromaticity components,
(c) Colourised chromaticity components by our method NLTV_CB

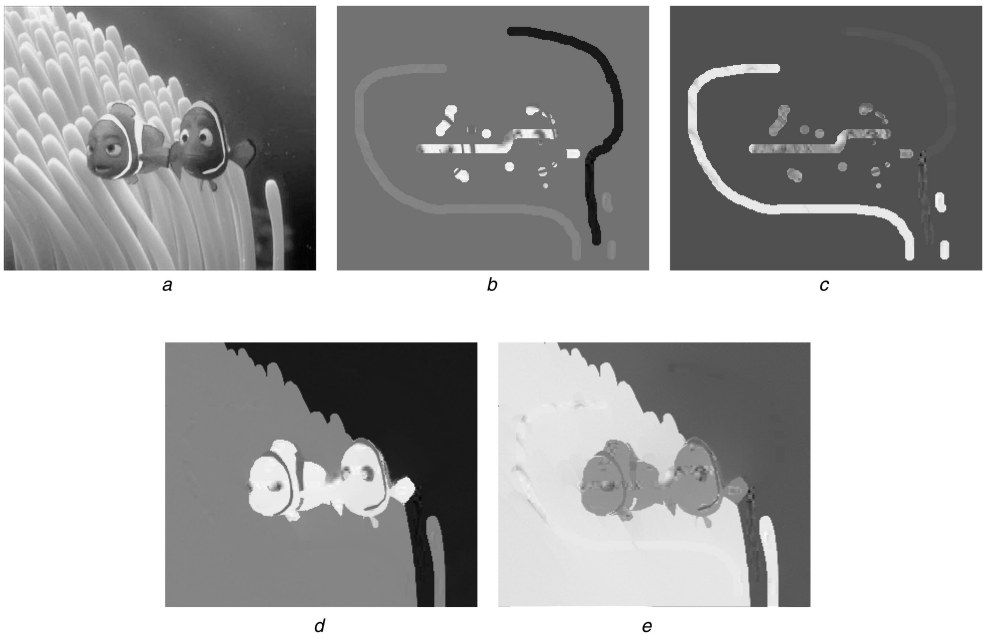

Fig. 11 *Intermediate colourisation results of the proposed method NLTV_YIQ on Nemo image*
(a) Given ***Y*** channel, ***(b)***, ***(c)*** Initial ***I*** and ***Q*** channels of the marked images, respectively,
(e), ***(f)*** Colourised ***I*** and ***Q*** channels by our method NLTV_YIQ, respectively

for 1000 iterations. As a limitation, our method appears to be much more time consuming than methods in [9, 19]. We remark that the proposed algorithms can speed up by including some parallel computing techniques. We leave it as our future work.

6 Conclusion

In this paper, we propose two new colourisation methods based on NLTV in the CB colour space and YIQ colour space, respectively. The non-local weight is computed by the known brightness/ luminance channel B or Y. The advantage of the proposed methods is that they are good at preserving the edges of colour in the process of colourisation. The proposed methods can be extended to other colour spaces in which the luminance information and colour information can be separated. The basic idea is using the luminance channel to guide the interpolation of colour channels. In the future work, we will consider other regularisation techniques in order to enhance both the image colourisation quality and the computational efficiency.

7 Acknowledgments

This work was supported by the National Science Foundation of China (11671002) and the Science and Technology Commission of Shanghai Municipality (STCSM) (13dz2260400).

8 References

[1] Fornasier, M.: 'Nonlinear projection digital image inpainting and restoration methods', *J. Math. Imaging Vis.*, 2006, **24**, (3), pp. 359–373
[2] Reinhard, E., Ashikhmin, M., Gooch, B., *et al.*: 'Color transfer between images', *IEEE Comput. Graph. Appl.*, 2001, **21**, (5), pp. 34–41
[3] Welsh, T., Ashikhmin, M., Mueller, K.: 'Transferring color to grayscale images', *Proc. ACM SIGGRAPH Conf.*, 2002, **21**, (3), pp. 277–280
[4] Gupta, R.K., Chia, A.Y.-S., Rajan, D., *et al.*: 'Image colorization using similar images'. Proc. of the 20th ACM Int. Conf. Multimedia, 2012, pp. 369–378
[5] Pan, Z., Dong, Z., Zhang, M.: 'A new algorithm for adding color to video or animation clips'. Proc. WSCG, Int. Conf. in Central Europe on Computer Graphics, Visualization and Computer Vision, 2004, pp. 515–519
[6] Madeira, J.S., Stork, A., Gros, M.H.: 'An approach to computer supported cartooning', *Vis. Comput.*, 1996, **12**, (1), pp. 1–17
[7] Horiuchi, T.: 'Colorization algorithm for gray-level image by probabilistic relaxation'. Proc. Int. Conf. Pattern Recognition, 2003, pp. 867–870
[8] Yatziv, L., Sapiro, G.: 'Fast image video colorization using blending', *IEEE Trans. Image Process.*, 2006, **15**, (5), pp. 1120–1129
[9] Levin, A., Lischinski, D., Weiss, Y.: 'Colorization using optimization', *Proc. ACM SIGGRAPH Conf.*, 2004, **23**, (3), pp. 689–694
[10] Kang, S.H., March, R.: 'Variational models for image colorization via chromaticity and brightness decomposition', *IEEE Trans. Image Process.*, 2007, **16**, (9), pp. 2251–2261
[11] Uruma, K., Konishi, K., Takahashi, T., *et al.*: 'Image colorization algorithm using series approximated sparse function'. IEEE Int. Conf. Acoustic, Speech and Signal Processing, 2014, pp. 1215–1219
[12] Lagodzinski, P., Smolka, B.: 'Fast digital image colorization technique'. IEEE Int. Symp. Signal Processing and Information Technology, 2007, pp. 813–818
[13] Krishnan, D., Szeliski, R.: 'Multigrid and multilevel preconditioners for computational photography', *ACM Trans. Graph. (TOG)*, 2011, **30**, (6), p. 177
[14] Uruma, K., Konishi, K., Takahashi, T., *et al.*: 'Image colorization based on the mixed L_0/L_1 norm minimization'. IEEE Int. Conf. Image Processing (ICIP), 2012, pp. 2113–2116
[15] Lee, S., Park, S.-W., Oh, P., *et al.*: 'Colorization-based compression using optimization', *IEEE Trans. Image Process.*, 2013, **22**, (7), pp. 2627–2636
[16] Mishiba, K., Yoshitome, T.: 'Colorization matrix construction with high compression efficiency for colorization-based coding using optimization'. IEEE Int. Conf. Image Processing (ICIP), 2014, 2014, pp. 5551–5555
[17] Pang, J., Au, O.C., Yamashita, Y., *et al.*: 'Self-similarity-based image colorization'. 2014 IEEE Int. Conf. Image Processing (ICIP), 2014, pp. 4687–4691
[18] Hua, M., Bie, X., Zhang, M., *et al.*: 'Edge-aware gradient domain optimization framework for image filtering by local propagation'. Proc. of the IEEE Conf. Computer Vision and Pattern Recognition, 2014, pp. 2838–2845
[19] Li, F., Bao, Z., Liu, R., *et al.*: 'Fast image inpainting and colorization by Chambolle's dual method', *J. Vis. Commun. Image Represent.*, 2011, **22**, (6), pp. 529–542
[20] Gonzalez, R.C., Woods, R.E.: 'Digital image processing'. 2002
[21] Gilboa, G., Osher, S.: 'Nonlocal operators with applications to image processing', *Multiscale Model. Simul.*, 2008, **7**, (3), pp. 1005–1028
[22] Bresson, X.: 'A short note for nonlocal tv minimization'. 2009, available at: http://www.cs.cityu.edu.hk/xbresson/ucla/index.html
[23] Zhang, X., Chan, T.F.: 'Wavelet inpainting by nonlocal total variation', *Inverse Probl. Imaging*, 2010, **4**, (1), pp. 191–210
[24] Zhang, X., Burger, M., Bresson, X., *et al.*: 'Bregmanized nonlocal regularization for deconvolution and sparse reconstruction', *SIAM J. Imaging Sci.*, 2010, **3**, (3), pp. 253–276
[25] Chambolle, A.: 'An algorithm for total variation minimization and applications', *J. Math. Imaging Vis.*, 2004, **20**, (1-2), pp. 89–97
[26] Chan, T.F., Golub, G.H., Mulet, P.: 'A nonlinear primal-dual method for total variation-based image restoration', *SIAM J. Sci. Comput.*, 1999, **20**, (6), pp. 1964–1977
[27] Fan, K.: 'Minimax theorems', *Proc. Natl. Acad. Sci. USA*, 1953, **39**, (1), p. 42
[28] Jack, K.: 'Video demystified: a handbook for the digital engineer', Newnes, 2005